

FedNorm: Modality-Based Normalization in Federated Learning for Multi-Modal Liver Segmentation

Tobias Bernecker^{1,2}, Annette Peters¹, Christopher L. Schlett³, Fabian Bamberg³, Fabian Theis¹, Daniel Rueckert², Jakob Weiß³ and Shadi Albarqouni^{1,2,4,†}

¹ *Helmholtz Zentrum München, Neuherberg, Germany*

² *Technical University of Munich, Garching, Germany*

³ *Medical Center-University of Freiburg, University of Freiburg, Freiburg, Germany*

⁴ *University Hospital Bonn, University of Bonn, Bonn, Germany*

† *Corresponding Author: (e-mail: shadi.albarqouni@ukbonn.de)*

Editor:

Abstract

Given the high incidence and effective treatment options for liver diseases, they are of great socioeconomic importance. One of the most common methods for analyzing CT and MRI images for diagnosis and follow-up treatment is liver segmentation. Recent advances in deep learning have demonstrated encouraging results for automatic liver segmentation. Despite this, their success depends primarily on the availability of an annotated database, which is often not available because of privacy concerns. Federated Learning has been recently proposed as a solution to alleviate these challenges by training a shared global model on distributed clients without access to their local databases. Nevertheless, Federated Learning does not perform well when it is trained on a high degree of heterogeneity of image data due to multi-modal imaging, such as CT and MRI, and multiple scanner types. To this end, we propose **FedNorm** and its extension **FedNorm+**, two Federated Learning algorithms that use a modality-based normalization technique. Specifically, **FedNorm** normalizes the features on a client-level, while **FedNorm+** employs the modality information of single slices in the feature normalization. Our methods were validated using 428 patients from six publicly available databases and compared to state-of-the-art Federated Learning algorithms and baseline models in heterogeneous settings (multi-institutional, multi-modal data). The experimental results demonstrate that our methods show an overall acceptable performance, achieve Dice per patient scores up to 0.961, consistently outperform locally trained models, and are on par or slightly better than centralized models.

1. Introduction

Liver cancer is the second most common cause of cancer deaths in the world with 830,180 in 2020 according to the Global Cancer Observatory (Global Cancer Observatory). Liver diseases such as hepatic steatosis, liver fibrosis as well as primary and secondary malignancies are of great socioeconomic importance given their high incidence and effective treatment options (Asrani et al., 2019). Thus, early diagnosis is desirable to reduce morbidity and mortality. Recent advanced in artificial intelligence, deep learning in particular, have shown encouraging results for automatic detection and quantification of these conditions. Such models are often trained in a supervised fashion, which requires a large amount of

pixel-wise annotated data (Ronneberger et al., 2015; Sun et al., 2017). Collecting ground-truth annotation is oftentimes time-consuming, tedious, and labor expensive. Besides, such a large database might not be available in a single institute or hospital due to the low incidence rate of pathological cases (Li et al., 2019).

A straightforward approach to overcome the aforementioned challenges would be to train a model on a collection of available training data (data lake) from multiple institutions. However, sharing sensitive data is often not possible, especially in the medical sector, due to data protection laws (Li et al., 2019) such as the General Data Protection Regulation ¹. Therefore, it would be helpful to train a shared global model in a decentralized fashion based on the available training data from multiple hospitals and institutes.

In 2017, McMahan et al. (McMahan et al., 2017) introduced the concept of Federated Learning (FL) where they demonstrated that training of a shared global model can be performed in a decentralized way, which overcomes the problem of data sharing. Since then, multiple works focused on heterogeneity in FL (Andreux et al., 2020; Bakhtiari et al., 2020; Hsu et al., 2020, 2019; Li et al., 2020a, 2021; Zhao et al., 2018). FL provides an adequate solution for training deep learning models with data coming from multiple institutions, especially in privacy-sensitive domains like medical imaging (Kaissis et al., 2021, 2020; Li et al., 2019, 2020c; Sheller et al., 2020). In this context, additional focus was placed on privacy-preserving FL (Kaissis et al., 2021, 2020; Li et al., 2019, 2020c). Nevertheless, FL was already used to train models for medical image segmentation, in many cases for brain tumor segmentation (Li et al., 2019; Sheller et al., 2020).

However, training a shared global model for medical image segmentation in a federated fashion poses several challenges. These include training deep learning models on multiple imaging modalities with a large number of scanners from different manufacturers, various image resolutions and protocols. This data can be seen as not independent and identically distributed (non-IID) (Wang et al., 2020). Furthermore, there is an imbalance of abundant annotated computed tomography (CT) scans and rarely annotated magnetic resonance imaging (MRI) scans, due to differences in acquisition times and costs (Oliva and Saini, 2004; Yang et al., 2019). For this reason, the CT and MRI segmentation performance could benefit from training a model on both imaging modalities (Valindria et al., 2018). In the past, multiple works focused on training liver/organ segmentation models on scans from multi-modal (CT and MRI) data (Valindria et al., 2018; Wang et al., 2019; Yang et al., 2019), on different MRI sequences (Couteaux et al., 2021) or for multi-modal liver lesion segmentation (Xue et al., 2021). Other works propose methods that are trained on one modality and can generalize to the other modality using domain adaptation (Chen et al., 2020; Jiang and Veeraraghavan, 2020; Yang et al., 2019). However, many works only focus on liver/organ segmentation on a single modality (Chen et al., 2012; Christ et al., 2016; Isensee et al., 2018; Li et al., 2018; Lu et al., 2017; Milletari et al., 2016), or propose methods that perform well for both imaging modalities, but are trained and tested separately for each modality (Christ et al., 2017; Mulay et al., 2020).

In this work, we aim to answer the question whether deep learning models can be trained on CT and MRI data for multi-modal liver segmentation in a federated fashion. To this end, we present two novel FL approaches, **FedNorm** and **FedNorm+**, which are based on the

1. <http://data.europa.eu/eli/reg/2016/679/oj>. (Accessed: 2021-05-29)

Mode Normalization (MN) (Deecke et al., 2018) technique and inspired by the Federated Averaging with Server Momentum (**FedAvgM**) (Hsu et al., 2019) algorithm. To the best of our knowledge, this work is the first work to train liver segmentation models on multi-modal data with FL. In our experiments, we compare **FedNorm** and **FedNorm+** to baselines and other state-of-the-art FL algorithms.

Even if privacy preservation plays a key role in FL with medical data (Kaissis et al., 2021, 2020; Li et al., 2019, 2020c), this work rather focuses on overcoming the problem of training deep learning models for multi-modal liver segmentation in a decentralized fashion, by reaching similar or better performance than models trained on data lakes.

The rest of this paper has the following structure. Section 2 gives an overview about different approaches for multi-modal liver segmentation and FL algorithms, which are designed to tackle the problem of data heterogeneity (Wang et al., 2020) in FL. Section 3 introduces our new approach, **FedNorm**, and its extension, **FedNorm+**, for multi-modal liver segmentation with FL. In Section 4, the datasets used in this work are presented. Furthermore, our experiments are explained in more detail and the corresponding results are shown. Finally, conclusions are drawn in Section 5.

2. Related Work

This work focuses on multi-modal liver segmentation on CT and MRI data with FL. Hence, this section highlights the research areas of multi-modal liver/organ segmentation on CT and MRI data, and FL with data heterogeneity (Wang et al., 2020) by presenting relevant methods in more detail.

Multi-Modal Liver Segmentation Training deep learning models with scans from multiple modalities, e.g. CT and MRI, can be challenging due to the domain shift between the modalities caused by differences in the scanners and protocols, which are used to acquire the medical images (see Section 3.1) (Yang et al., 2019). On the other hand, training a model on scans from multiple modalities increases the amount of available training data, which may not be available in sufficient quantity for a specific modality, and leads to a better segmentation performance on the single modalities (Valindria et al., 2018). In this sense an early work used an encoder-decoder network to extract shared information from unpaired CT and MRI scans to perform multi-modal organ segmentation (Valindria et al., 2018). Another method uses transfer learning to refine an initial model, which is pre-trained on a single modality, for CT and MRI liver segmentation (Wang et al., 2019). Usually, domain adaptation can be used to overcome the problem of domain shift between CT and MRI data. To this end, one approach proposes to learn disentangled representations in an unsupervised way to separate the content and style representations of CT and MRI scans (Yang et al., 2019). Afterwards, a U-Net (Ronneberger et al., 2015) is trained for the task of liver segmentation on generated content-only images of the respective CT and MRI scans (Yang et al., 2019). However, all of these approaches train the networks in a centralized fashion and require both modalities during training. Therefore, they are not applicable to real-world FL settings, where both modalities may not be available at each client. Nevertheless, the pre-trained model from the transfer learning approach of Wang et al. (Wang et al., 2019) can be refined on single modalities. In this work, we train multi-modal liver segmentation models with FL, where each client only needs to have data from one modality, but may have

data from both modalities. Thus, our methods can be applied to scenarios with real-world hospitals.

Federated Learning with Data Heterogeneity FedAvg (McMahan et al., 2017), the base algorithm for FL, can achieve a good performance on heterogeneous data settings (McMahan et al., 2017). It may, however, show a performance degradation on non-IID data (Zhao et al., 2018). Nevertheless, FedAvg can converge to the optimum under certain circumstances when applied to these tasks (Li et al., 2020b). To avoid this performance degradation and to prevent parameters from oscillating, the FedAvgM algorithm (Hsu et al., 2019) uses momentum-based updates in the aggregation step of the server (Hsu et al., 2019). However, it is very sensitive to the choice of the momentum parameter and learning rate (Hsu et al., 2019). In contrast, we propose to use an interpolation between the old state and new averaged state only of specific parameters, e.g. only of the normalization parameters in the network (see Section 3.2.1), as these parameters are the critical part. If the normalization works as intended, the other parameters should get refined to the same optimum by all clients.

Federated Virtual Clients (FedVC) (Hsu et al., 2020) is an algorithm that solves the problem of different sizes of training datasets at each client. Therefore, it limits the number of local client updates to be the same for each client and selects clients with a probability based on their amount of training samples (Hsu et al., 2020). One drawback of FedVC is that clients with rare samples of data, but a low training dataset size are less likely to get selected and therefore may be neglected during FL. Our approaches, however, are based on the example of FedAvg, where each client performs the full number of local updates and gets selected with equal probability.

Recent works propose to use Batch Normalization (BN) (Ioffe and Szegedy, 2015) to address the problem of data heterogeneity in FL: The SiloBN (Andreux et al., 2020) algorithm keeps the BN statistics (μ and σ) local at each client to learn a specific model for each client. FedBN (Li et al., 2021), on the other hand, keeps the BN parameters (γ and β) and statistics (μ and σ) local at each client, to tackle the problem of feature distribution shift among data from different clients (Li et al., 2021). Due to the missing BN statistics in the shared global models of SiloBN and FedBN, generalization to unseen data/clients requires to compute these statistics first (Andreux et al., 2020; Li et al., 2021). Additionally, the shared global model of FedBN does not contain the BN parameters (Li et al., 2021). For this reason, FedBN requires access to these parameters from other/all clients inside the federation when it gets tested on unseen data (Li et al., 2021). We, however, identify latent modes within each modality of the data. Thus, we use the MN technique (Deecke et al., 2018), an extension of BN that normalizes the data according to multiple modes (Deecke et al., 2018), in our approaches. Our global model shares all network parameters and thus does not share the limitations of SiloBN and FedBN.

3. Methodology

In this section, we present our proposed approaches for multi-modal liver segmentation on CT and MRI data with FL. Therefore, we first identify some challenges and define important design requirements that we consider in our approaches. Finally, we introduce our approaches, FedNorm and its extension FedNorm+.

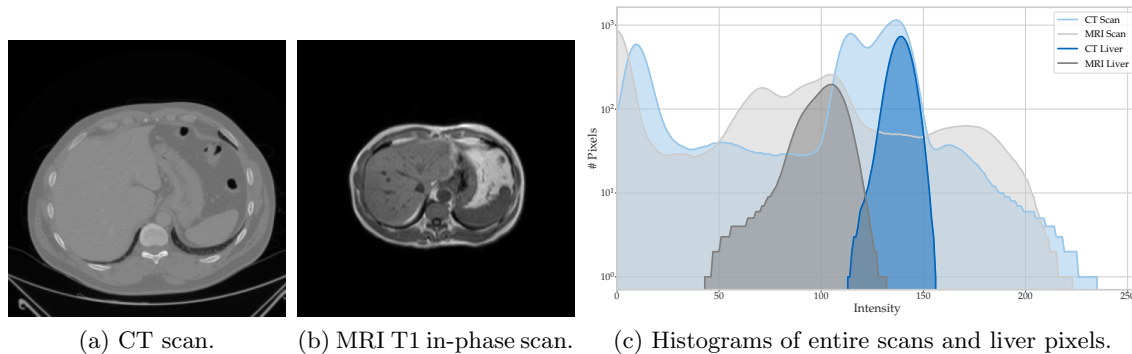


Figure 1: CT (a) and MRI (b) scans from the CHAOS19 (Kavur et al., 2019) dataset together with histograms of the whole scans and the liver pixels only (c). Figure inspired by Yang et al. (Yang et al., 2019, Fig. 1).

3.1 Challenges and Design Requirements

Due to the high level of data heterogeneity (Wang et al., 2020) among the datasets of the clients in the federation, the task of multi-modal liver segmentation with FL includes multiple challenges. These challenges comprise, but are not limited to: 1) Data from different modalities at the clients, i.e. clients with only CT, only MRI, or data from both modalities. 2) Unbalanced amounts of data at different clients. This may include unbalanced amounts of CT and MRI data at clients with data from both modalities. 3) The scans are recorded with different scanners and protocols, and therefore have different image resolutions, sizes and spacing between slices. Additionally, scans coming from different imaging modalities have different visual appearances (see Figure 1).

In this work, the aim is to solve these challenges by introducing own approaches. In addition, the developed approaches should overcome the limitations of previous methods (see Section 2). To this end, we formulate a list of key design requirements, which we consider when developing our algorithms: 1) Avoid heavy pre-processing steps, e.g. disentangled representations used in the work of Yang et al. (Yang et al., 2019). 2) No need of having both modalities per client (reflects a real-world scenario). 3) Deal with multi-modal data inside the federation and, if necessary, per client. 4) Handle unbalanced amounts of data per client. 5) Keep the number of model parameters low. 6) Direct applicability of the learned global model to unseen data/clients.

According to the design requirements above, solving the problem of data heterogeneity and multi-modal data inside the federation is the main challenge of this work. Due to multiple causes, such as different scanners, protocols, resolutions or appearances, a domain shift occurs between both modalities (Yang et al., 2019). This domain shift can be observed in Figure 1, which shows the histograms of the entire scans and the liver pixels only of a CT and a MRI scan. It can be seen that the intensity histograms of the entire scans cover the same area, but are quite dissimilar. The histograms of the liver pixels, cover different intensities, which poses a challenge for liver segmentation algorithms. For this reason, we decided to use the concept of MN (Deecke et al., 2018) in our proposed approaches because

it is able to capture different modes in the data, which can be identified in Figure 1, and to normalize the data accordingly.

3.2 Federated Learning with Modality-Based Normalization

In this work, we propose two FL algorithms, which leverage the MN technique (Deecke et al., 2018) and normalize data based on their modality information. Specifically, MN is a normalization technique and an extension of BN (Ioffe and Szegedy, 2015). Inspired by the idea that samples inside a dataset/minibatch belong to different latent modes with shared common features, Deecke et al. (Deecke et al., 2018) propose to separately normalize samples within a minibatch based on these modes, instead of normalizing all the samples in the minibatch based on the same mean and variance as in BN (Ioffe and Szegedy, 2015). Therefore, MN considers M modes and uses a set of gating functions $\{g_m\}_{m=1}^M$, where each function determines, how likely a sample belongs to mode $m \in \{1, \dots, M\}$. Due to the functionality of our algorithms, we term the first **FedNorm** and its extension **FedNorm+**. Both algorithms are explained in more detail in the following.

3.2.1 FEDNORM

While other FL algorithms consider all parameters of all selected clients per round to get averaged at the server, e.g. **FedAvg** (McMahan et al., 2017), **FedNorm** separates between normalization parameters, i.e. all parameters and statistics from all MN layers in the neural network, and non-normalization parameters, i.e. all other parameters. The normalization parameters are further divided into CT and MRI modalities, and the server needs to know whether a client contains only CT data or only MRI data. Each modality has its own MN parameters and statistics $\boldsymbol{\theta}^{(\text{modality})} := \bigcup_{l \text{ is MN}} \{\boldsymbol{\alpha}^{(l)}, \boldsymbol{\beta}^{(l)}, \overline{\langle \mathbf{x} \rangle}^{(l)}, \overline{\langle \mathbf{x}^2 \rangle}^{(l)}\}$ with M modes, respectively, which contain all parameters ($\boldsymbol{\alpha}$ and $\boldsymbol{\beta}$) and statistics ($\overline{\langle \mathbf{x} \rangle}$ and $\overline{\langle \mathbf{x}^2 \rangle}$) from all MN layers in the network. This allows the neural network to find latent modes within each modality. When distributing the global model parameters to the clients in round t , the server sends the non-normalization parameters $\boldsymbol{\theta}_t$ together with the normalization parameters $\boldsymbol{\theta}_t^{(\text{CT})}$ for a client with CT data, or $\boldsymbol{\theta}_t^{(\text{MRI})}$ for a client with MRI data. Based on the received parameters $\boldsymbol{\theta} = \{\boldsymbol{\theta}_t, \boldsymbol{\theta}_t^{(\text{modality})}\}$, each client performs local training on its own data for E epochs. In the aggregation step, the server averages the non-normalization parameters $\boldsymbol{\theta}_{t+1}^{(k)}$ from all selected clients $k \in S_t$ of the current round t in the same way as **FedAvg** (McMahan et al., 2017). The CT and MRI normalization parameters and statistics of the MN layers are averaged separately and depending on their modality. Additionally, inspired by the **FedAvgM** algorithm (Hsu et al., 2019), the aim is to avoid oscillations in the parameter updates. Different from **FedAvgM**, **FedNorm** uses $\beta \in (0, 1]$ to interpolate between the old state of the normalization parameters and the new averaged normalization parameters. The intention of the separation of normalization parameters into CT and MRI modalities is to normalize the data within these MN layers to similar states and therefore use the same non-normalization parameters for both modalities. Hence, the interpolation mechanism is only used to update the normalization parameters and is not needed for the non-normalization parameters. A detailed description of **FedNorm** can be found in Algorithm 1.

Algorithm 1 FedNorm. K is the total number of clients, k is the index of one client, T is the number of FL rounds, B is the local minibatch size, E is the number of local epochs, $C \in (0, 1]$ is the fraction of clients selected in each FL round, η is the local learning rate, \mathcal{L} is a loss function, \mathcal{D}_k is the dataset of client k , $N_k = |\mathcal{D}_k|$ is the number of samples in dataset \mathcal{D}_k , and β is the interpolation ratio. Algorithm partially adapted from McMahan et al. (McMahan et al., 2017, Algorithm 1).

```

1: Server executes:
2: Initialize  $\theta_1, \theta_1^{(\text{CT})}, \theta_1^{(\text{MRI})}$ 
3: for round  $t = 1$  to  $T$  do
4:    $m \leftarrow \max(C \cdot K, 1)$ 
5:    $S_t \leftarrow$  (random set of  $m$  clients)
6:   for each client  $k \in S_t$  in parallel do
7:     if modality(client  $k$ ) == CT then
8:        $\{\theta_{t+1}^{(k)}, \theta_{t+1,k}^{(\text{CT})}\} \leftarrow$  ClientUpdate( $k, \{\theta_t, \theta_t^{(\text{CT})}\}$ )
9:     else if modality(client  $k$ ) == MRI then
10:       $\{\theta_{t+1}^{(k)}, \theta_{t+1,k}^{(\text{MRI})}\} \leftarrow$  ClientUpdate( $k, \{\theta_t, \theta_t^{(\text{MRI})}\}$ )
11:    $N \leftarrow \sum_{k \in S_t} N_k$ 
12:   // Aggregate non-normalization parameters:
13:    $\theta_{t+1} \leftarrow \sum_{k \in S_t} \frac{N_k}{N} \theta_{t+1}^{(k)}$ 
14:   // Aggregate normalization parameters:
15:   for modality  $\in \{\text{CT}, \text{MRI}\}$  do
16:      $\theta_{t+1}^{(\text{modality})} \leftarrow (1 - \beta) \theta_t^{(\text{modality})} + \beta \sum_{k \in S_t} \frac{N_k}{N} \theta_{t+1,k}^{(\text{modality})}$ 
17: ClientUpdate( $k, \theta$ ): // Run on client  $k$ 
18:    $\mathcal{B} \leftarrow$  (split  $\mathcal{D}_k$  into batches of size  $B$ )
19:   for epoch  $i = 1$  to  $E$  do
20:     for batch  $b \in \mathcal{B}$  do
21:        $\theta \leftarrow \theta - \eta \nabla \mathcal{L}(b; \theta)$ 
22:   return  $\theta$ 

```

3.2.2 FEDNORM+

FedNorm separates the MN parameters and statistics by modalities and distributes these parameters to the clients based on the modality of their data. As a consequence, it cannot handle mixed-modality clients, which contain CT and MRI data, and thus would not be applicable to real-world scenarios. For this reason, we propose FedNorm+, an extension of FedNorm, which does not separate between normalization and non-normalization parameters. Instead, it only uses one set of MN parameters and statistics, which is distributed to all selected clients per round in the same way as in FedAvg (McMahan et al., 2017). For the MN layers, the number of modes is fixed to $M = 2$ with the intention to capture and normalize the samples of each modality (CT and MRI) with one mode, respectively. Therefore, the modality information of each scan is handed to the network and forwarded to each MN layer. Based on this information, the respective mode is chosen in a hard-coded way (cf. original MN technique (Deecke et al., 2018)):

- Mode 1 (CT): Set $g_1(\mathbf{x}_n) = 1 \wedge g_2(\mathbf{x}_n) = 0$ if modality(\mathbf{x}_n) = CT

- Mode 2 (MRI): Set $g_1(\mathbf{x}_n) = 0 \wedge g_2(\mathbf{x}_n) = 1$ if $\text{modality}(\mathbf{x}_n) = \text{MRI}$

Consequently, the parameters for each modality are trained on their respective scans. In the aggregation step, **FedNorm+** uses the same parameter aggregation as **FedAvg** (McMahan et al., 2017) for all parameters. Due to the hard-coded mode assignment, the parameters and statistics for each mode (modality) of a MN layer are aggregated separately. Additionally, the interpolation mechanism of **FedNorm** with momentum β is used to update all parameters, instead of only the MN parameters and statistics, to avoid oscillations in the updates.

4. Experiments and Results

To validate the performance of our proposed approaches, we perform multiple experiments with different FL settings and datasets. We aim to answer the following questions related to data heterogeneity: *i) How well do the models perform when each client only contains data from a single modality?* *ii) What happens if CT only, MRI only, and mixed-modality (CT + MRI) clients participate in the training?* To address these questions, we carefully designed our Non-IID 1 setting (three CT and three MRI clients) for (i) and our Non-IID 2 setting (two CT, two MRI, and two mixed-modality clients) for (ii).

4.1 Datasets

In our experimental settings, we use multiple publicly available CT and MRI datasets: LiTS17 (Bilic et al., 2019), the 3D-IRCADb-01 dataset of 3D-IRCADb (3DI) (included in the training set of LiTS17), abdominal scans from the Multi-Atlas dataset (Landman et al., 2013), SLIVER07 (Heimann et al., 2009), and CHAOS19 (Kavur et al., 2019). Furthermore, we use a random subset of 207 T1-weighted MRI scans (patients) from the KORA in-house dataset (KOR). Detailed information including technical specifications, e.g. numbers of patients (volumes), resolution, modalities, and demographics for all datasets can be found in Table 1. Here, we only use the training sets from LiTS17, Multi-Atlas, SLIVER07, and CHAOS19, for which the ground truth liver segmentation masks are provided. For CHAOS19, we compute water-only and fat-only images based on the T1-weighted in-phase and out-phase scans from CHAOS19 using the Dixon technique (Dixon, 1984) with the formulas provided in Ma (Ma, 2008).

We cropped (left and right in axial view) the scans from the KORA dataset (KOR) and padded them with zeros (top and bottom in axial view) to obtain images of size 256×256 pixels. Furthermore, we removed many, but not all, slices that do not contain the liver. Consequently, the models can be trained to predict a segmentation for the liver only on images on which it is present.

The scans in the other datasets have varying image sizes (see Table 1) and intensity value ranges. Therefore, the scans are first resized to a size of 256×256 pixels and the intensity values of the 2D slices are normalized based on the single scalar mean and standard deviation values that are obtained by taking the mean and standard deviation of all intensities per slice and taking the mean over all slices from all volumes in the dataset. Resizing the CT scans from 512×512 pixels to 256×256 pixels also has the effect of doubling their image resolution (x - y -plane), resulting in approximately the same image resolution as the MRI

Table 1: Technical and demographic information about the liver segmentation datasets used in this work. ”# Sites” indicates the number of institutions from which the data was acquired. ”# Slices/Patient” gives a range with the minimum and maximum number of slices per patient. The age and liver size are reported with mean and standard deviation. The resolution (physical size) of a voxel is given in x -, y -, and z -direction, where the latter corresponds to the space between neighboring slices.

Feature	LiTS17 Bilic et al. (2019)	w/o 3D-IRCADb	3D-IRCADb 3DI	Multi-Atlas Landman et al. (2013)	SLIVER07 Heimann et al. (2009)	CHAOS19 Kavur et al. (2019) CT	CHAOS19 Kavur et al. (2019) MRI	KORA KOR
# Sites	6	1	Multiple	Multiple	Multiple	1	1	Multiple
# Patients	111	20	30	20	20	20	20	207
# Slices	55815	2823	3779	4159	2874	647 (T1), 623 (T2)	21379	21379
# Slices/Patient	[75, 987]	[74, 260]	[85, 198]	[64, 294]	[81, 266]	[26, 50]	[73, 138]	[73, 138]
Modality	CT	CT	CT	CT	CT	MRI	MRI	MRI
Health Status	Most scans with tumors, e.g. HCC	75% with liver tumors	n.a.	Most scans with tumors/metastasis/cysts	healthy	healthy	healthy	and (pre-)diabetic
Age (years)	n.a.	53.6 ± 13.4	n.a.	n.a.	n.a.	n.a.	n.a.	56.2 ± 9.3
# Women/Men	n.a.	10/10	n.a.	n.a.	n.a.	n.a.	n.a.	98/109
Image Size	512 × 512	512 × 512	512 × 512	512 × 512	512 × 512	512 × 512	{256, 280, 320} ²	256 × 256
Scanner	Multiple	n.a.	Multiple	Multiple	Multiple	n.a.	1.5T Philips MRI	3T Siemens Skyra
Resolution (mm)	{0.56, 0.98} × {0.7, 3.0}	{0.56, 0.87} × {1.0, 4.0}	{0.59, 0.98} × {0.59, 0.98} × {2.5, 5.0}	{0.58, 0.81} × {0.58, 0.81} × {0.7, 3.0}	{0.57, 0.79} × {0.57, 0.79} × {1.0, 2.0}	{1.36, 2.03} × {1.36, 2.03} × {5.5, 9.0}	{1.67, 1.74} × {1.67, 1.74}	{1.7, 1.7} × {1.67, 1.74} × {1.67, 1.74}
Liver Size (cm ³)	1694.398 ± 406.093	1583.721 ± 272.122	1738.907 ± 446.85	1710.61 ± 434.628	1592.109 ± 281.597	1609.635 ± 500.653	1608.312 ± 376.634	

scans. Finally, the normalized values are clipped to $[-3, 3]$ as proposed by Stan et al. (Stan and Rostami, 2021).

4.2 Experiments

Table 2: Experimental FL settings based on data from the Multi-Atlas Landman et al. (2013), 3D-IRCADb 3DI, SLIVER07 Heimann et al. (2009), CHAOS19 Kavur et al. (2019), LiTS17 Bilic et al. (2019), and KORA KOR datasets. The last three columns indicate the splitting of the volumes (patients) in the datasets of the clients into training, validation and testing parts. For each client dataset, a standalone local model is trained as an upper bound baseline. Furthermore, a centralized model for each setting is trained on the collection of training data (data lake) from all clients in the setting.

Setting	Models	Datasets	Modality	# Training Volumes	# Validation Volumes	# Testing Volumes
Non-IID 1	Clients/ Local Models	Multi-Atlas	CT	8	4	18
		3D-IRCADb	CT	8	4	8
		SLIVER07	CT	8	4	8
		CHAOS19 MR T1 In-Phase	MRI	8	4	8
		CHAOS19 MR T1 Out-Phase	MRI	8	4	8
		CHAOS19 MR T1 Water	MRI	8	4	8
	Centralized Model	All Clients	CT + MRI	48	24	58
Non-IID 2	Clients/ Local Models	Multi-Atlas	CT	8	4	18
		3D-IRCADb	CT	8	4	8
		CHAOS19 MR T1 Water	MRI	8	4	8
		KORA T1 Water (1)	MRI	8	4	8
		SLIVER07 + KORA T1 Water (2)	CT + MRI	16 (8 + 8)	8 (4 + 4)	16 (8 + 8)
		LiTS17 Site 2 + KORA T1 Water (3)	CT + MRI	14 (6 + 8)	7 (3 + 4)	14 (6 + 8)
	Centralized Model	All Clients	CT + MRI	62	31	72

We use two different experimental FL settings to train, validate and test our proposed approaches, FedNorm (Section 3.2.1) and FedNorm+ (Section 3.2.2), and compare them against baselines and other state-of-the-art methods. Specifically, we design two non-IID settings, which contain clients with datasets from both modalities and which cover different scenarios: The Non-IID 1 setting contains a balanced number of CT and MRI clients, where the dataset of each client only contains data from one modality. The Non-IID 2 setting in-

cludes CT, MRI and mixed-modality (CT + MRI) clients. However, the Non-IID 1 setting is biased in the MRI clients because all of them show the same patients (shapes), but in different MRI sequences (appearances). Specifically, the designed FL settings contain an increasing amount of data heterogeneity (Wang et al., 2020) from the Non-IID 1 to the Non-IID 2 setting, due to the mixed-modality clients. Detailed information about both FL settings is provided in Table 2. Here, the clients correspond to different hospitals, each with its own training, validation and testing sets from one (or two) dataset(s), and thus with specific scanner types and protocols per client, which were used to record the medical images. For the client datasets, we mainly use a splitting of 40% - 20% - 40% (instead of the more common 80% - 10% - 10%) because FL aggregates the client models, which in turn is similar to training on an aggregation of the training sets from the clients. Another reason for this partitioning of the data is to have as few patients as possible per client for training, to reflect a real-world scenario with rarely labeled volumes in each hospital, and to have as many volumes as possible for testing. To evaluate the performance of the models, we use the Dice coefficient (Dice, 1945).

4.2.1 MODEL SELECTION

Before comparing our proposed approaches to other methods, we select winners for **FedNorm** (Section 3.2.1) and **FedNorm+** (Section 3.2.2) by tuning their hyper-parameters. Here, we follow the proposal of Sheller et al. (Sheller et al., 2020) and select a winner based on the highest global validation score reported during training. According to Sheller et al. (Sheller et al., 2020), this global validation score is computed by aggregating the local validation scores of all clients in the federation, which validate the global model at the beginning of each round on their local validation set before starting their training. However, we do not include all clients for training in each round, but we compute the global validation score based on the local validation scores of all clients in the federation. Therefore, we compute the mean (instead of a weighted average based on the amount of client data) of local validation scores to obtain the global validation score. Consequently, the validation score of each client contributes equally to the global score, which then measures the overall performance on the data of all clients.

FedNorm For **FedNorm**, we focus on the number of modes M per modality and the interpolation ratio β , which is used for aggregating the averaged new and old normalization parameters, as hyper-parameters. For this reason, we investigate the influence of $M \in \{1, 2, 3, 4\}$ and $\beta \in \{1.0, 0.9, 0.5, 0.2\}$, where the old state of the normalization parameters is ignored with $\beta = 1.0$, and $\beta = 0.2$ only slightly changes the old normalization parameters in the direction of the averaged new ones. To this end, we train **FedNorm** with each combination of M and β for 100 FL rounds with two clients per round and $E = 1$ local epoch on the Non-IID 1 setting (see Table 2) because it is the only setting which **FedNorm** can handle. The highest global validation Dice scores for all combinations within these 100 FL rounds of training are reported in Table 3. Based on these scores, we select **FedNorm** with $M = 2$ modes and $\beta = 0.9$ as the winner and use it in our further experiments.

FedNorm+ Since the number of modes is fixed to $M = 2$ for **FedNorm+** (see Section 3.2.2), we only focus on the interpolation ratio β as a hyper-parameter. Similar to **FedNorm**, we investigate the influence of $\beta \in \{1.0, 0.9, 0.5, 0.2\}$. Therefore, we train **FedNorm+** for 100 FL

Table 3: Highest global validation Dice scores for FedNorm and FedNorm+ with different interpolation ratios β and varying numbers of modes M per modality reported within 100 FL rounds of training on the Non-IID 1 (FedNorm) and Non-IID 2 (FedNorm+) settings. The best global validation Dice score per method is highlighted in bold.

Method	# Modes (M)	Interpolation Ratio (β)			
		1.0	0.9	0.5	0.2
FedNorm	1	0.889	0.880	0.880	0.860
	2	0.892	0.893	0.889	0.863
	3	0.888	0.889	0.882	0.868
	4	0.889	0.885	0.880	0.840
FedNorm+	2	0.876	0.877	0.879	0.831

rounds with two clients per round and $E = 1$ local epoch on the Non-IID 2 setting (see Table 2) because it is our FL setting with the highest degree of data heterogeneity (Wang et al., 2020).

The highest global validation Dice scores within the 100 FL rounds of training are reported in Table 3. Based on these values, we select FedNorm+ with $\beta = 0.5$ as the winner and use it in our further experiments.

4.2.2 IMPLEMENTATION DETAILS

Due to the great success of the U-Net (Ronneberger et al., 2015) neural network architecture in biomedical image segmentation, we employ a shallower version of the original network for the task of liver segmentation on 2D slices in this work. Here, we reduce the feature map channels of the original U-Net (Ronneberger et al., 2015) from $\{64, 128, 256, 512, 1024\}$ to $\{8, 16, 32, 64\}$, resulting in $\sim 136\text{K}$ instead of $\sim 36\text{M}$ parameters. Consequently, this modified version of the U-Net meets the desired requirement to keep the number of model parameters low (see Section 3.1). The final (1×1) convolution of our modified U-Net computes an output with only one channel, followed by the sigmoid function (Bishop, 2006, Equation 4.59) to compute a pixel-wise pseudo-probability for each pixel, which tells how likely it belongs to the liver.

Furthermore, zero-padding of size one is used to obtain the same output size as the input size for the 3×3 convolutions.

For the state-of-the-art FL algorithms, FedAvg (McMahan et al., 2017), FedAvgM (Hsu et al., 2019), FedVC (Hsu et al., 2020), SiLoBN (Andreux et al., 2020), and FedBN (Li et al., 2021), we use our own re-implementation based on the information in these works to better fit our needs and code framework. For the experiments with FedAvg, FedAvgM, FedVC, and the local models (see Table 2), we use our modified version of the U-Net. For FedAvgM, we set the momentum parameter to $\beta = 0.6$ in both settings. The number of local updates S in FedVC is limited to the minimum number of training samples (slices) among all K clients in the federation divided by the batch size B (cf. Hsu et al. (Hsu et al., 2020)), $S = \lfloor \min\{N_1, \dots, N_K\} / B \rfloor$, where N_k is the training dataset size of client k . For SiLoBN and FedBN, BN (Ioffe and Szegedy, 2015) layers are inserted between each convolution layer

and Rectified Linear Unit (ReLU) into our modified version of the U-Net, except for the last convolution layer. For **FedNorm** (Section 3.2.1), **FedNorm+** (Section 3.2.2), and the centralized models (see Table 2), MN (Deecke et al., 2018) layers instead of BN layers are inserted at the same position into our modified U-Net. Here, we use MN with $M = 2$ for all **FedNorm** experiments (see Section 4.2.1). For the centralized models, we use MN with $M = 4$ modes in the modified U-Net of the Non-IID 1 setting (because **FedNorm** has M modes for each of the two modalities) and MN with $M = 2$ modes for the Non-IID 2 setting to guarantee a fair comparison to **FedNorm** and **FedNorm+** (see Section 4.2.1). We take the implementation of MN from publicly available code ² from Deecke et al. (Deecke et al., 2018).

The training of all local and centralized models, and at each client for the FL algorithms was performed with the Adam optimizer (Kingma and Ba, 2015) with a learning rate of $\eta = 0.001$ and a batch size of $B = 12$. All local and centralized models are trained for 50 epochs with possible early stopping after a patience of five epochs. We train the models on both FL settings (see Table 2) for $T = 100$ FL rounds. In each round, two clients are sampled randomly, but fixed to be the same for all FL algorithms. Inspired by the work of Zhao et al. (Zhao et al., 2018), we train a neural network for $E = 1$ local epoch at the client side to prevent a large divergence of the federated global model parameters from parameters that the centralized model would learn. Our code is made publicly available ³.

All models are trained in a supervised fashion to minimize a total loss. Inspired by Isensee et al. (Isensee et al., 2018), this total loss is composed of the Dice loss (Milletari et al., 2016) and the cross-entropy loss (Bishop, 2006). Specifically, we use the binary cross-entropy (BCE) loss (Bishop, 2006, cf. Equation 4.90) \mathcal{L}_{BCE} for two classes. Hence, the total loss is $\mathcal{L} = \mathcal{L}_{\text{Dice}} + \mathcal{L}_{\text{BCE}}$ (cf. Isensee et al. (Isensee et al., 2018, Equation 1)). However, different from the Dice loss proposed by Milletari et al. (Milletari et al., 2016), we use the non-binary pseudo-probabilities $p_{ij} \in [0, 1]$ instead of binary segmentations to compute the loss value (cf. Kodym et al. (Kodym et al., 2019)). Nevertheless, binary segmentation results are used to compute the Dice coefficient (Dice, 1945) values in the evaluation, where we round the non-binary predictions p_{ij} of the network to binary values: $\hat{y}_{ij} = 0$, if $p_{ij} \in [0, 0.5]$, and $\hat{y}_{ij} = 1$, if $p_{ij} \in (0.5, 1]$.

4.2.3 COMPARISON WITH BASELINES AND STATE OF THE ART

We compare **FedNorm** (Section 3.2.1) and **FedNorm+** (Section 3.2.2) to different baselines and state-of-the-art FL algorithms in both FL settings (see Table 2). As baselines, we consider local models and centralized models. The local models are trained on the training set of each client, individually. Consequently, the performance of these models can be seen as upper bounds for each client dataset. Additionally, per setting, we train one centralized model on the collection of training data (data lake) from all clients in the setting. Specifically, Table 2 gives the number of training, validation and testing volumes (patients) for all FL clients, local and centralized models in each setting.

As state-of-the-art FL algorithms, we choose the base FL algorithm, **FedAvg** (McMahan et al., 2017), and different approaches, which tackle the problem of data heterogeneity (Wang

2. <https://github.com/ldeecke/mn-torch> (Accessed: 2021-08-28)

3. <https://github.com/albarqounilab/FedNorm>

et al., 2020) in FL, to compare against **FedNorm** and **FedNorm+**: **FedAvgM** (Hsu et al., 2019), **FedVC** (Hsu et al., 2020), **SiloBN** (Andreux et al., 2020), and **FedBN** (Li et al., 2021). For all FL algorithms, the global model from the server aggregation of the last FL round is sent back to each client and is tested on the test set of each client without any refinement. To compare the different methods, we measure the performance of all models on the test sets of all clients in both settings (Table 2) with the Dice coefficient (Dice, 1945). The resulting performance values for both settings are shown in Table 4 and will be investigated in further detail in the following. To indicate the difference in performance between the federated and centralized models, and the local models, the relative improvement (RI) (Kravchenko and Bullock, 1999) is computed as $RI = \frac{x_2 - x_1}{x_1} \cdot 100\%$ (Kravchenko and Bullock, 1999, cf. Equation 9), which gives the improvement (in percent) of performance score x_2 over score x_1 , where both are measured with the same metric. Additionally, the unpaired two-sided t-test is performed on the Dice per patient results of the local model and each federated or centralized model, respectively, where a p -value ≤ 0.05 indicates statistical significance.

In Table 4 it can be seen that the federated models consistently (except for CHAOS19 MR T1 Out-Phase and Water) outperform the local models (positive RI). Furthermore, in many cases, the performances of some federated models are similar or even better than the ones from the centralized models, which use more volumes, coming from both modalities, directly for model training. Additionally, it can be seen that **FedNorm** and **FedNorm+** show the best performance per client in many cases and outperform the centralized models on most of the client’s test sets. Furthermore, it has to be noted that the model from **FedNorm+** is the only model that can outperform the local model on the CHAOS19 MR T1 Water client in the Non-IID 2 setting, and by a large margin.

Overall, it can be observed that Dice per patient scores up to 0.961 for CT and up to 0.941 for MRI are reached on the client test sets. Hence, these results demonstrate that our proposed method for multi-modal liver segmentation can be trained successfully on CT and MRI data with FL, by achieving a high performance.

To confirm these observations, a visual comparison of the performances of the local models, **FedBN**, **FedNorm+**, and the centralized model on the test sets of the clients in the Non-IID 2 setting is presented in Figure 2, as **FedBN** can be identified as one of the strongest competitors to **FedNorm+** according to Table 4. It can be seen that the model of **FedNorm+** shows a good performance, where the local models fail and even where **FedBN** and the centralized model do not provide precise liver segmentations. It also shows that **FedNorm+** is able to accurately segment the liver even in unfamiliar appearances (KORA T1 Water (1) client) and that it does not falsely segment areas with similar intensity values as the liver, like the other models on the Multi-Atlas client.

5. Conclusion

Based on our experimental results, we conclude that our proposed FL methods for multi-modal liver segmentation can be trained on data from multiple modalities (e.g. CT and MRI) by reaching a high performance. We have observed that the federated models in our experiments consistently outperform local models, which are trained on each dataset individually. Furthermore, in some cases, the federated models have also outperformed the centralized models. This demonstrates that it is not necessary to collect data from multiple

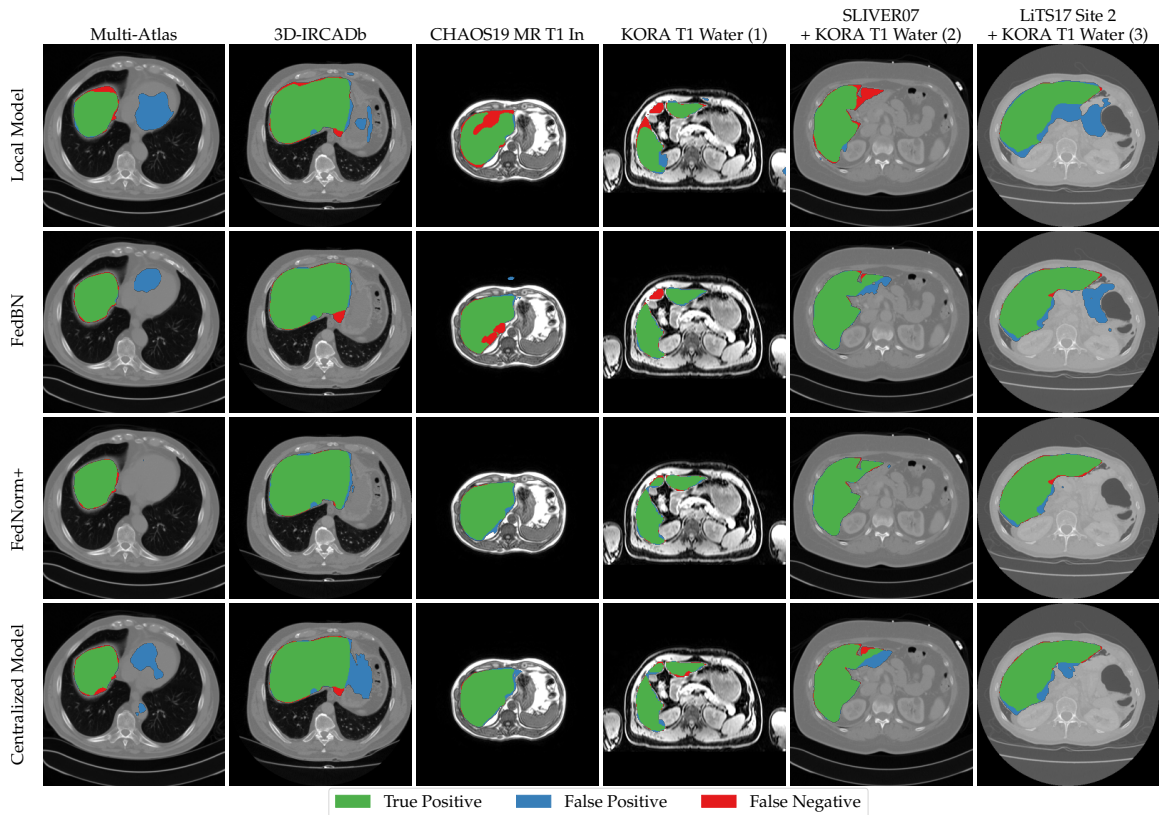


Figure 2: Comparison of visual results of the liver segmentation predictions from the local models, FedBN, FedNorm+, and the centralized model (rows) on one slice from the test set of each client (columns) of the Non-IID 2 setting.

hospitals and modalities at a central location (data lake) to train deep learning models for multi-modal liver segmentation on CT and MRI data. It is rather sufficient to have a few participating clients (hospitals) inside the federation during FL, where each client contains data from either only CT/MRI, or both modalities. We have further observed that our approaches outperform other state-of-the-art FL algorithms for most of the clients in our FL settings. However, the problem of FedNorm is that it cannot handle clients with data from both modalities. To this end, we have proposed FedNorm+, which normalizes the data based on slice-wise modality information and a hard-coded mode assignment. According to our results, it is also sufficient to use a relatively small version of the U-Net (Ronneberger et al., 2015) to achieve high performances for multi-modal liver segmentation.

References

3D-IRCADb. <https://www.ircad.fr/research/3dircadb/>. (Accessed: 2021-01-07).

Kooperative Gesundheitsforschung in der Region Augsburg (KORA). <https://www.helmholtz-muenchen.de/en/kora/index.html>. (Accessed: 2021-05-21).

- Mathieu Andreux, Jean Ogier du Terrail, Constance Beguier, and Eric W. Tramel. Siloed federated learning for multi-centric histopathology datasets. In Shadi Albarqouni, Spyridon Bakas, Konstantinos Kamnitsas, M. Jorge Cardoso, Bennett Landman, Wenqi Li, Fausto Milletari, Nicola Rieke, Holger Roth, Daguang Xu, and Ziyue Xu, editors, *Domain Adaptation and Representation Transfer, and Distributed and Collaborative Learning*, pages 129–139, Cham, 2020. Springer International Publishing. ISBN 978-3-030-60548-3. doi: https://doi.org/10.1007/978-3-030-60548-3_13.
- Sumeet K. Asrani, Harshad Devarbhavi, John Eaton, and Patrick S. Kamath. Burden of liver diseases in the world. *Journal of Hepatology*, 70(1):151–171, 2019. ISSN 0168-8278. doi: <https://doi.org/10.1016/j.jhep.2018.09.014>.
- Mohammad Bakhtiari, Reza Nasirigerdeh, Reihaneh Torkzadehmahani, Amirhossein Bayat, David B. Blumenthal, Markus List, and Jan Baumbach. Federated multi-mini-batch: An efficient training approach to federated learning in non-iid environments, 2020.
- Patrick Bilic, Patrick Ferdinand Christ, Eugene Vorontsov, Grzegorz Chlebus, Hao Chen, Qi Dou, Chi-Wing Fu, Xiao Han, Pheng-Ann Heng, Jürgen Hesser, Samuel Kadoury, Tomasz Konopczynski, Miao Le, Chunming Li, Xiaomeng Li, Jana Lipková, John Lowengrub, Hans Meine, Jan Hendrik Moltz, Chris Pal, Marie Piraud, Xiaojuan Qi, Jin Qi, Markus Rempfler, Karsten Roth, Andrea Schenk, Anjany Sekuboyina, Eugene Vorontsov, Ping Zhou, Christian Hülsemeyer, Marcel Beetz, Florian Ettl, Felix Gruen, Georgios Kaissis, Fabian Lohöfer, Rickmer Braren, Julian Holch, Felix Hofmann, Wieland Sommer, Volker Heinemann, Colin Jacobs, Gabriel Efrain Humpire Mamani, Bram van Ginneken, Gabriel Chartrand, An Tang, Michal Drozdal, Avi Ben-Cohen, Eyal Klang, Marianne M. Amitai, Eli Konen, Hayit Greenspan, Johan Moreau, Alexandre Hostettler, Luc Soler, Refael Vivanti, Adi Szeskin, Naama Lev-Cohain, Jacob Sosna, Leo Joskowicz, and Bjoern H. Menze. The liver tumor segmentation benchmark (lits), 2019.
- Christopher M. Bishop. *Pattern Recognition and Machine Learning (Information Science and Statistics)*. Springer-Verlag, Berlin, Heidelberg, 2006. ISBN 0387310738.
- Cheng Chen, Qi Dou, Hao Chen, Jing Qin, and Pheng Ann Heng. Unsupervised bidirectional cross-modality adaptation via deeply synergistic image and feature alignment for medical image segmentation. *IEEE Transactions on Medical Imaging*, 39(7):2494–2505, 2020. doi: [10.1109/TMI.2020.2972701](https://doi.org/10.1109/TMI.2020.2972701).
- Yufei Chen, Zhicheng Wang, Jinyong Hu, Weidong Zhao, and Qidi Wu. The domain knowledge based graph-cut model for liver ct segmentation. *Biomedical Signal Processing and Control*, 7(6):591–598, 2012. ISSN 1746-8094. doi: <https://doi.org/10.1016/j.bspc.2012.04.005>. Biomedical Image Restoration and Enhancement.
- Patrick Ferdinand Christ, Mohamed Ezzeldin A. Elshaer, Florian Ettl, Sunil Tatavarty, Marc Bickel, Patrick Bilic, Markus Rempfler, Marco Armbruster, Felix Hofmann, Melvin D’Anastasi, Wieland H. Sommer, Seyed-Ahmad Ahmadi, and Bjoern H. Menze. Automatic liver and lesion segmentation in ct using cascaded fully convolutional neural networks and 3d conditional random fields. In Sebastien Ourselin, Leo Joskowicz,

- Mert R. Sabuncu, Gozde Unal, and William Wells, editors, *Medical Image Computing and Computer-Assisted Intervention – MICCAI 2016*, pages 415–423, Cham, 2016. Springer International Publishing. ISBN 978-3-319-46723-8. doi: https://doi.org/10.1007/978-3-319-46723-8_48.
- Patrick Ferdinand Christ, Florian Ettliger, Felix Grün, Mohamed Ezzeldin A. Elshaera, Jana Lipkova, Sebastian Schlecht, Freba Ahmaddy, Sunil Tatavarty, Marc Bickel, Patrick Bilic, Markus Rempfler, Felix Hofmann, Melvin D Anastasi, Seyed-Ahmad Ahmadi, Georgios Kaissis, Julian Holch, Wieland Sommer, Rickmer Braren, Volker Heinemann, and Bjoern Menze. Automatic liver and tumor segmentation of ct and mri volumes using cascaded fully convolutional neural networks, 2017.
- Vincent Couteaux, Mathilde Trintignac, Olivier Nempont, Guillaume Pizaine, Anna Sesilia Vlachomitrou, Pierre-Jean Valette, Laurent Milot, and Isabelle Bloch. Comparing deep learning strategies for paired but unregistered multimodal segmentation of the liver in t1 and t2-weighted mri, 2021.
- Lucas Deecke, Iain Murray, and Hakan Bilen. Mode normalization, 2018. International Conference on Learning Representations (2019).
- Lee R. Dice. Measures of the amount of ecologic association between species. *Ecology*, 26(3):297–302, 1945. doi: <https://doi.org/10.2307/1932409>. URL <https://esajournals.onlinelibrary.wiley.com/doi/abs/10.2307/1932409>.
- WT Dixon. Simple proton spectroscopic imaging. *Radiology*, 153(1):189–194, October 1984. ISSN 0033-8419. doi: 10.1148/radiology.153.1.6089263. URL <https://doi.org/10.1148/radiology.153.1.6089263>.
- Global Cancer Observatory. World Fact Sheets. <https://gco.iarc.fr/today/data/factsheets/populations/900-world-fact-sheets.pdf>, 2021. (Accessed: 2021-05-29).
- Tobias Heimann, Bram van Ginneken, Martin A. Styner, Yulia Arzhaeva, Volker Aurich, Christian Bauer, Andreas Beck, Christoph Becker, Reinhard Beichel, GyÖrgy Bekes, Fernando Bello, Gerd Binnig, Horst Bischof, Alexander Bornik, Peter M. M. Cashman, Ying Chi, Andrés Cordova, Benoit M. Dawant, Márta Fidrich, Jacob D. Furst, Daisuke Furukawa, Lars Grenacher, Joachim Hornegger, Dagmar Kainmüller, Richard I. Kitney, Hidefumi Kobatake, Hans Lamecker, Thomas Lange, Jeongjin Lee, Brian Lennon, Rui Li, Senhu Li, Hans-Peter Meinzer, GÁbor Nemeth, Daniela S. Raicu, Anne-Mareike Rau, Eva M. van Rikxoort, MikaËl Rousson, LÁszló Rusko, Kinda A. Saddi, GÜnter Schmidt, Dieter Seghers, Akinobu Shimizu, Pieter Slagmolen, Erich Sorantin, Grzegorz Soza, Ruchaneewan Susomboon, Jonathan M. Waite, Andreas Wimmer, and Ivo Wolf. Comparison and evaluation of methods for liver segmentation from ct datasets. *IEEE Transactions on Medical Imaging*, 28(8):1251–1265, 2009. doi: 10.1109/TMI.2009.2013851.
- Tzu-Ming Harry Hsu, Hang Qi, and Matthew Brown. Measuring the effects of non-identical data distribution for federated visual classification, 2019.

- Tzu-Ming Harry Hsu, Hang Qi, and Matthew Brown. Federated visual classification with real-world data distribution. In Andrea Vedaldi, Horst Bischof, Thomas Brox, and Jan-Michael Frahm, editors, *Computer Vision – ECCV 2020*, pages 76–92, Cham, 2020. Springer International Publishing. ISBN 978-3-030-58607-2. doi: https://doi.org/10.1007/978-3-030-58607-2_5.
- Sergey Ioffe and Christian Szegedy. Batch normalization: Accelerating deep network training by reducing internal covariate shift. In Francis Bach and David Blei, editors, *Proceedings of the 32nd International Conference on Machine Learning*, volume 37 of *Proceedings of Machine Learning Research*, pages 448–456, Lille, France, Jul 2015. PMLR.
- Fabian Isensee, Jens Petersen, Andre Klein, David Zimmerer, Paul F. Jaeger, Simon Kohl, Jakob Wasserthal, Gregor Koehler, Tobias Norajitra, Sebastian Wirkert, and Klaus H. Maier-Hein. nnu-net: Self-adapting framework for u-net-based medical image segmentation, 2018.
- Jue Jiang and Harini Veeraraghavan. Unified cross-modality feature disentangler for unsupervised multi-domain mri abdomen organs segmentation. In Anne L. Martel, Purang Abolmaesumi, Danail Stoyanov, Diana Mateus, Maria A. Zuluaga, S. Kevin Zhou, Daniel Racoceanu, and Leo Joskowicz, editors, *Medical Image Computing and Computer Assisted Intervention – MICCAI 2020*, pages 347–358, Cham, 2020. Springer International Publishing. ISBN 978-3-030-59713-9. doi: https://doi.org/10.1007/978-3-030-59713-9_34.
- Georgios Kaissis, Alexander Ziller, Jonathan Passerat-Palmbach, Théo Ryffel, Dmitrii Usynin, Andrew Trask, Ionésio Lima, Jason Mancuso, Friederike Jungmann, Marc-Matthias Steinborn, Andreas Saleh, Marcus Makowski, Daniel Rueckert, and Rickmer Braren. End-to-end privacy preserving deep learning on multi-institutional medical imaging. *Nature Machine Intelligence*, 3(6):473–484, Jun 2021. ISSN 2522-5839. doi: [10.1038/s42256-021-00337-8](https://doi.org/10.1038/s42256-021-00337-8). URL <https://doi.org/10.1038/s42256-021-00337-8>.
- Georgios A. Kaissis, Marcus R. Makowski, Daniel Rückert, and Rickmer F. Braren. Secure, privacy-preserving and federated machine learning in medical imaging. *Nature Machine Intelligence*, 2(6):305–311, Jun 2020. ISSN 2522-5839. doi: [10.1038/s42256-020-0186-1](https://doi.org/10.1038/s42256-020-0186-1). URL <https://doi.org/10.1038/s42256-020-0186-1>.
- Ali Emre Kavur, M. Alper Selver, Oğuz Dicle, Mustafa Barış, and N. Sinem Gezer. CHAOS - Combined (CT-MR) Healthy Abdominal Organ Segmentation Challenge Data, Apr 2019. URL <https://doi.org/10.5281/zenodo.3362844>.
- Diederik P. Kingma and Jimmy Ba. Adam: A method for stochastic optimization. In Yoshua Bengio and Yann LeCun, editors, *3rd International Conference on Learning Representations, ICLR 2015, San Diego, CA, USA, May 7-9, 2015, Conference Track Proceedings*, 2015.
- Oldřich Kodým, Michal Španěl, and Adam Herout. Segmentation of head and neck organs at risk using cnn with batch dice loss. In Thomas Brox, Andrés Bruhn, and Mario Fritz, editors, *Pattern Recognition*, pages 105–114, Cham, 2019. Springer International Publishing. ISBN 978-3-030-12939-2.

- Alexandra Kravchenko and Donald G. Bullock. A comparative study of interpolation methods for mapping soil properties. *Agronomy Journal*, 91(3):393–400, 1999. doi: <https://doi.org/10.2134/agronj1999.00021962009100030007x>.
- Bennett Landman, Zhoubing Xu, Juan Eugenio Igelsias, Martin Styner, Thomas Robin Langerak, and Arno Klein. Multi-Atlas Labeling Beyond the Cranial Vault - Workshop and Challenge. <https://www.synapse.org/#!/Synapse:syn3193805/wiki/89480>, 2013. (Accessed: 2021-01-03).
- Tian Li, Anit Kumar Sahu, Manzil Zaheer, Maziar Sanjabi, Ameet Talwalkar, and Virginia Smith. Federated optimization in heterogeneous networks. In I. Dhillon, D. Papailiopoulos, and V. Sze, editors, *Proceedings of Machine Learning and Systems*, volume 2, pages 429–450, 2020a.
- Wenqi Li, Fausto Milletari, Daguang Xu, Nicola Rieke, Jonny Hancox, Wentao Zhu, Maximilian Baust, Yan Cheng, Sébastien Ourselin, M. Jorge Cardoso, and Andrew Feng. Privacy-preserving federated brain tumour segmentation. In Heung-Il Suk, Mingxia Liu, Pingkun Yan, and Chunfeng Lian, editors, *Machine Learning in Medical Imaging*, pages 133–141, Cham, 2019. Springer International Publishing. ISBN 978-3-030-32692-0. doi: https://doi.org/10.1007/978-3-030-32692-0_16.
- Xiang Li, Kaixuan Huang, Wenhao Yang, Shusen Wang, and Zhihua Zhang. On the convergence of fedavg on non-iid data. In *International Conference on Learning Representations*, 2020b. URL <https://openreview.net/forum?id=HJxNAnVtDS>.
- Xiaomeng Li, Hao Chen, Xiaojuan Qi, Qi Dou, Chi-Wing Fu, and Pheng-Ann Heng. Hdenseunet: Hybrid densely connected unet for liver and tumor segmentation from ct volumes. *IEEE Transactions on Medical Imaging*, 37(12):2663–2674, 2018. doi: 10.1109/TMI.2018.2845918.
- Xiaoxiao Li, Yufeng Gu, Nicha Dvornek, Lawrence H. Staib, Pamela Ventola, and James S. Duncan. Multi-site fmri analysis using privacy-preserving federated learning and domain adaptation: Abide results. *Medical Image Analysis*, 65:101765, 2020c. ISSN 1361-8415. doi: <https://doi.org/10.1016/j.media.2020.101765>.
- Xiaoxiao Li, Meirui JIANG, Xiaofei Zhang, Michael Kamp, and Qi Dou. FedBN: Federated learning on non-IID features via local batch normalization. In *International Conference on Learning Representations*. OpenReview.net, 2021. URL <https://openreview.net/forum?id=6YEQUn0QICG>.
- Fang Lu, Fa Wu, Peijun Hu, Zhiyi Peng, and Dexing Kong. Automatic 3d liver location and segmentation via convolutional neural networks and graph cut. *International Journal of Computer Assisted Radiology and Surgery*, 12(2):171–182, Feb 2017. ISSN 1861-6429. doi: 10.1007/s11548-016-1467-3.
- Jingfei Ma. Dixon techniques for water and fat imaging. *Journal of Magnetic Resonance Imaging*, 28:543 – 558, 09 2008. doi: 10.1002/jmri.21492.

- Brendan McMahan, Eider Moore, Daniel Ramage, Seth Hampson, and Blaise Agueria y Arcas. Communication-Efficient Learning of Deep Networks from Decentralized Data. In Aarti Singh and Jerry Zhu, editors, *Proceedings of the 20th International Conference on Artificial Intelligence and Statistics*, volume 54 of *Proceedings of Machine Learning Research*, pages 1273–1282. PMLR, Apr 2017.
- Fausto Milletari, Nassir Navab, and Seyed-Ahmad Ahmadi. V-net: Fully convolutional neural networks for volumetric medical image segmentation. In *2016 Fourth International Conference on 3D Vision (3DV)*, pages 565–571, 2016. doi: 10.1109/3DV.2016.79.
- Supriti Mulay, G. Deepika, S. Jeevakala, Keerthi Ram, and Mohanasankar Sivaprakasam. Liver segmentation from multimodal images using hed-mask r-cnn. In Quanzheng Li, Richard Leahy, Bin Dong, and Xiang Li, editors, *Multiscale Multimodal Medical Imaging*, pages 68–75, Cham, 2020. Springer International Publishing. ISBN 978-3-030-37969-8. doi: https://doi.org/10.1007/978-3-030-37969-8_9.
- Maria Raquel Oliva and Sanjay Saini. Liver cancer imaging: role of ct, mri, us and pet. *Cancer imaging*, 4 Spec No A:42–46, Apr 2004. ISSN 1470-7330. doi: 10.1102/1470-7330.2004.0011.18215974[pmid].
- Olaf Ronneberger, Philipp Fischer, and Thomas Brox. U-net: Convolutional networks for biomedical image segmentation. In Nassir Navab, Joachim Hornegger, William M. Wells, and Alejandro F. Frangi, editors, *Medical Image Computing and Computer-Assisted Intervention – MICCAI 2015*, pages 234–241, Cham, 2015. Springer International Publishing. ISBN 978-3-319-24574-4.
- Micah Sheller, Brandon Edwards, G. Reina, Jason Martin, Sarthak Pati, Aikaterini Kotrotsou, Mikhail Milchenko, Weilin Xu, Daniel Marcus, Rivka Colen, and Spyridon Bakas. Federated learning in medicine: facilitating multi-institutional collaborations without sharing patient data. *Scientific Reports*, 10, 07 2020. doi: 10.1038/s41598-020-69250-1.
- Serban Stan and Mohammad Rostami. Privacy preserving domain adaptation for semantic segmentation of medical images, 2021.
- Chen Sun, Abhinav Shrivastava, Saurabh Singh, and Abhinav Gupta. Revisiting unreasonable effectiveness of data in deep learning era. In *2017 IEEE International Conference on Computer Vision (ICCV)*, pages 843–852, 2017. doi: 10.1109/ICCV.2017.97.
- Vanya V. Valindria, Nick Pawlowski, Martin Rajchl, Ioannis Lavdas, Eric O. Aboagye, Andrea G. Rockall, Daniel Rueckert, and Ben Glocker. Multi-modal learning from unpaired images: Application to multi-organ segmentation in ct and mri. In *2018 IEEE Winter Conference on Applications of Computer Vision (WACV)*, pages 547–556, 2018. doi: 10.1109/WACV.2018.00066. © 2011 IEEE.
- Kang Wang, Adrija Mamidipalli, Tara Retson, Naeim Bahrami, Kyle Hasenstab, Kevin Blansit, Emily Bass, Timoteo Delgado, Guilherme Cunha, Michael Middleton, Rohit Loomba, Brent Neuschwander-Tetri, Claude Sirlin, and Albert Hsiao. Automated ct and mri liver segmentation and biometry using a generalized convolutional neural network. *Radiology: Artificial Intelligence*, 1:180022, 03 2019. doi: 10.1148/ryai.2019180022.

- Yuanli Wang, Dhruv Kumar, and Abhishek Chandra. Poster: Exploiting data heterogeneity for performance and reliability in federated learning. In *2020 IEEE/ACM Symposium on Edge Computing (SEC)*, pages 164–166, 2020. doi: 10.1109/SEC50012.2020.00023.
- Zhongliang Xue, Ping Li, Liang Zhang, Xiaoyuan Lu, Guangming Zhu, Peiyi Shen, Syed Afaq Ali Shah, and Mohammed Bennamoun. Multi-modal co-learning for liver lesion segmentation on pet-ct images. *IEEE Transactions on Medical Imaging*, pages 1–1, 2021. doi: 10.1109/TMI.2021.3089702.
- Junlin Yang, Nicha C. Dvornek, Fan Zhang, Julius Chapiro, MingDe Lin, and James S. Duncan. Unsupervised domain adaptation via disentangled representations: Application to cross-modality liver segmentation. In Dinggang Shen, Tianming Liu, Terry M. Peters, Lawrence H. Staib, Caroline Essert, Sean Zhou, Pew-Thian Yap, and Ali Khan, editors, *Medical Image Computing and Computer Assisted Intervention – MICCAI 2019*, pages 255–263, Cham, 2019. Springer International Publishing. ISBN 978-3-030-32245-8. doi: https://doi.org/10.1007/978-3-030-32245-8_29.
- Yue Zhao, Meng Li, Liangzhen Lai, Naveen Suda, Damon Civin, and Vikas Chandra. Federated learning with non-iid data, 2018.

Table 4: Comparison on the Non-IID 1 and 2 settings. The numbers give the performances of the local models, the centralized model, and the federated global models (without refinement at the clients) on the test set of each client. The performances are reported with Dice per patient and are given by mean (median) and standard deviation. Additionally, the RI is computed for the mean Dice per patient of the models from the FL algorithms and the centralized models over the local model performances. The best score from the federated models per setting and client is highlighted in bold. Additionally, the unpaired two-sided t-test was performed using the Dice per patient scores from the local model against the results from each federated model and the centralized model per client. A star (*) behind respective RI value indicates statistical significance with a p -value ≤ 0.05 .

Methods	Non-IID 1			Non-IID 2		
	Client (Modality)	Dice per Patient \uparrow	RI \uparrow [%]	Client (Modality)	Dice per Patient \uparrow	RI \uparrow [%]
Local		0.850 (0.862) \pm 0.050	-		0.850 (0.862) \pm 0.050	-
FedAvg McMahan et al. (2017)		0.883 (0.899) \pm 0.071	3.9		0.906 (0.907) \pm 0.042	6.6*
FedAvgM Hsu et al. (2019)		0.575 (0.541) \pm 0.150	-32.4*		-	-
FedVC Hsu et al. (2020)		0.884 (0.885) \pm 0.036	4.0*		0.848 (0.843) \pm 0.056	-0.2
SiloBN Andreux et al. (2020)	Multi-Atlas (CT)	0.870 (0.909) \pm 0.117	2.4	Multi-Atlas (CT)	0.894 (0.895) \pm 0.045	5.2*
FedBN Li et al. (2021)		0.900 (0.921) \pm 0.053	5.9*		0.916 (0.919) \pm 0.034	7.8*
FedNorm		0.921 (0.932) \pm 0.033	8.4*		-	-
FedNorm+		0.891 (0.898) \pm 0.034	4.8*		0.916 (0.928) \pm 0.030	7.8*
Centralized		0.921 (0.934) \pm 0.033	8.4*		0.894 (0.914) \pm 0.061	5.2*
Local		0.918 (0.926) \pm 0.029	-		0.918 (0.926) \pm 0.029	-
FedAvg McMahan et al. (2017)		0.940 (0.942) \pm 0.018	2.4		0.933 (0.946) \pm 0.037	1.6
FedAvgM Hsu et al. (2019)		0.874 (0.888) \pm 0.036	-4.8*		-	-
FedVC Hsu et al. (2020)		0.929 (0.933) \pm 0.022	1.2		0.916 (0.916) \pm 0.024	-0.2
SiloBN Andreux et al. (2020)	3D-IRCADb (CT)	0.954 (0.958) \pm 0.014	3.9*	3D-IRCADb (CT)	0.961 (0.967) \pm 0.011	4.7*
FedBN Li et al. (2021)		0.954 (0.954) \pm 0.015	3.9*		0.960 (0.963) \pm 0.011	4.6*
FedNorm		0.956 (0.959) \pm 0.017	4.1*		-	-
FedNorm+		0.942 (0.942) \pm 0.016	2.6		0.955 (0.956) \pm 0.016	4.0*
Centralized		0.953 (0.957) \pm 0.012	3.8*		0.938 (0.945) \pm 0.028	2.2
Local		0.888 (0.887) \pm 0.062	-		0.718 (0.784) \pm 0.209	-
FedAvg McMahan et al. (2017)		0.888 (0.924) \pm 0.135	0.0		0.421 (0.472) \pm 0.339	-41.4
FedAvgM Hsu et al. (2019)		0.761 (0.785) \pm 0.122	-14.3*		-	-
FedVC Hsu et al. (2020)		0.905 (0.926) \pm 0.079	1.9		0.424 (0.493) \pm 0.277	-40.9*
SiloBN Andreux et al. (2020)	SLIVER07 (CT)	0.924 (0.944) \pm 0.070	4.1	CHAOS19 MR T1 Water (MRI)	0.514 (0.498) \pm 0.233	-28.4
FedBN Li et al. (2021)		0.906 (0.928) \pm 0.064	2.0		0.459 (0.512) \pm 0.319	-36.1
FedNorm		0.914 (0.940) \pm 0.084	2.9		-	-
FedNorm+		0.883 (0.903) \pm 0.116	-0.6		0.759 (0.754) \pm 0.065	5.7
Centralized		0.934 (0.943) \pm 0.057	5.2		0.893 (0.879) \pm 0.082	24.4
Local		0.254 (0.278) \pm 0.168	-		0.865 (0.870) \pm 0.043	-
FedAvg McMahan et al. (2017)		0.460 (0.511) \pm 0.233	81.1		0.930 (0.935) \pm 0.030	7.5*
FedAvgM Hsu et al. (2019)		0.579 (0.661) \pm 0.199	128.0*		-	-
FedVC Hsu et al. (2020)		0.228 (0.070) \pm 0.301	-10.2		0.893 (0.896) \pm 0.044	3.2
SiloBN Andreux et al. (2020)	CHAOS19 MR T1 In-Phase (MRI)	0.656 (0.678) \pm 0.185	158.3*	T1 Water (1) (MRI)	0.932 (0.933) \pm 0.026	7.7*
FedBN Li et al. (2021)		0.386 (0.485) \pm 0.333	52.0		0.941 (0.945) \pm 0.021	8.8*
FedNorm		0.795 (0.851) \pm 0.170	213.0*		-	-
FedNorm+		0.653 (0.803) \pm 0.303	157.1*		0.938 (0.941) \pm 0.022	8.4*
Centralized		0.688 (0.869) \pm 0.369	170.9*		0.936 (0.939) \pm 0.024	8.2*
Local		0.704 (0.735) \pm 0.182	-		0.703 (0.872) \pm 0.348	-
FedAvg McMahan et al. (2017)		0.443 (0.477) \pm 0.237	-37.1*		0.793 (0.928) \pm 0.282	12.8
FedAvgM Hsu et al. (2019)		0.590 (0.672) \pm 0.248	-16.2		-	-
FedVC Hsu et al. (2020)		0.296 (0.285) \pm 0.307	-58.0*		0.733 (0.886) \pm 0.333	4.3
SiloBN Andreux et al. (2020)	CHAOS19 MR T1 Out-Phase (MRI)	0.735 (0.713) \pm 0.137	4.4	SLIVER07 + KORA T1 Water (2) (CT + MRI)	0.823 (0.923) \pm 0.214	17.1
FedBN Li et al. (2021)		0.444 (0.460) \pm 0.358	-36.9		0.784 (0.927) \pm 0.282	11.5
FedNorm		0.777 (0.786) \pm 0.090	10.4		-	-
FedNorm+		0.661 (0.752) \pm 0.271	-6.1		0.755 (0.933) \pm 0.347	7.4
Centralized		0.716 (0.867) \pm 0.318	1.7		0.844 (0.925) \pm 0.165	20.1
Local		0.718 (0.784) \pm 0.209	-		0.885 (0.918) \pm 0.089	-
FedAvg McMahan et al. (2017)		0.481 (0.578) \pm 0.280	-33.0		0.932 (0.953) \pm 0.050	5.3
FedAvgM Hsu et al. (2019)		0.604 (0.672) \pm 0.240	-15.9		-	-
FedVC Hsu et al. (2020)		0.291 (0.248) \pm 0.311	-59.5*		0.882 (0.909) \pm 0.089	-0.3
SiloBN Andreux et al. (2020)	CHAOS19 MR T1 Water (MRI)	0.683 (0.685) \pm 0.164	-4.9	+ KORA T1 Water (3) (CT + MRI)	0.918 (0.942) \pm 0.070	3.7
FedBN Li et al. (2021)		0.467 (0.543) \pm 0.342	-35.0		0.810 (0.915) \pm 0.174	-8.5
FedNorm		0.807 (0.841) \pm 0.126	12.4		-	-
FedNorm+		0.680 (0.784) \pm 0.285	-5.3		0.942 (0.946) \pm 0.023	6.4*
Centralized		0.744 (0.893) \pm 0.317	3.6		0.938 (0.950) \pm 0.035	6.0